Dual-Resonance U-Shaped Wearable Antenna with T-Slot Ground for On-Body Biomedical Devices

Ashraf Abuelhaija¹, Mohammed Hamdan¹, Gameel Saleh², Sanaa Salama³, Samer Issa¹, Osama Nashwan¹, and Adel Ashyap⁴

¹Department of Electrical Engineering, Applied Science Private University, Amman, Jordan

²Biomedical Engineering Department, College of Engineering, Imam Abdulrahman Bin Faisal University,

P.O. Box 1982, Dammam, 31441, Saudi Arabia

³Department of Biomedical Engineering, Arab American University, Jenin, Palestine

⁴School of Electrical, Computer and Telecommunication Engineering, University of Wollongong,

Wollongong, NSW 2500, Australia

Corresponding author: Ashraf Abuelhaija (e-mail: a_abualhijaa@asu.edu.jo)

ABSTRACT This study introduces a miniaturized and adaptable dual-band textile antenna, meticulously designed for implementation in wearable biomedical systems. It functions at 2.45 GHz and 5.8 GHz, covering the ISM (Industrial, Scientific, and Medical) frequency ranges. The antenna features a U-shaped patch with a T-shaped slotted ground plane, built from denim fabric ($\varepsilon_r = 1.68$) and ShieldIt Super conductive material. Following several design optimizations—such as via placement, curvature conformity, and slot tuning—the final prototype shows reliable impedance matching (S11 < -10 dB across both bands) and consistent radiation performance, validated using CST and COMSOL simulations.

The antenna maintains dependable performance on the human body, with SAR levels staying within safe exposure thresholds (1.18 W/kg at 2.45 GHz and 1.44 W/kg at 5.8 GHz). Although radiation efficiency drops are observed when worn (approximately -10.5 dB and -15.6 dB at 2.45 GHz and 5.8 GHz respectively) due to body absorption, the radiation pattern remains directed and functional. These characteristics make the design well-suited for body-worn communication systems used in healthcare monitoring, fitness tracking, and military contexts. This flexible antenna meets safety and comfort requirements, offering a viable solution for WLAN/WBAN implementations in wearable technology.

INDEX TERMS Flexible antenna, dual-band operation, biomedical wearables, ISM bands, specific absorption rate, body-area networks

I. INTRODUCTION

EARABLE antennas constitute a critical component of Body-Centric Communication (BCC) systems, making them key elements in modern wireless communication advancements. Thanks to their distinctive electromagnetic behavior and adaptable design, these antennas have attracted significant research attention. A major area of focus is their application in Wireless Body Area Networks (WBANs), which facilitate data transfer between human physiology and electronic devices. These systems are used in diverse fields like mobile health monitoring, smart identification systems, biomedical diagnostics, and even sports performance tracking.In particular, wearable technologies are emerging as transformative tools in healthcare, aiming to minimize clinical errors and enhance the quality of care within medical institutions [1].

WBANs are generally deployed in close proximity to the human body, where they facilitate the acquisition and transmission of vital physiological parameters—such as cardiac activ-

ity, blood oxygen saturation, glucose levels, arterial pressure, and related biomarkers—to external medical instrumentation or clinical information systems for diagnostic and monitoring purposes. These technological advancements hold significant promise in medical environments, contributing to the mitigation of clinical inaccuracies and enhancing the overall standard of patient care [2]–[7].

The International Telecommunication Union (ITU) has assigned several frequency bands for medical communication applications [8], including the 402–405 MHz Medical Implant Communication Service (MICS) [9]. For instance, in the U.S., Wireless Medical Telemetry Services (WMTS) operate within 608–614 MHz, 1.395–1.4 GHz, and 1.429–1.432 GHz [10].

In addition, the ISM frequency bands — such as 2.42–2.48 GHz and 5.3–5.9 GHz — can be used license-free for medical devices due to their advantageous signal characteristics [11]. Lower frequencies (sub-100 MHz) are ideal for short-range, high-penetration communication, while ISM



and MICS support higher data throughput and more robust links [12]. In line with ISM and 5G wireless evolution, modern wearable antennas often operate at 2.45 GHz, 5.8 GHz, and nearby bands [13].

One key consideration in wearable antenna development is selecting flexible and comfortable substrates, since rigid materials can impair performance by reducing bandwidth and efficiency [14]–[16]. Many designs suffer from limitations like size constraints, reduced bandwidth, and strong signal absorption by human tissue. To address these, research has explored compact antenna layouts, such as slot-based and microstrip patch configurations, and refined them for better performance [17]–[20].

Improved matching techniques and surface wave suppression have also been introduced using various patch shapes [21], [22], and efforts have expanded antenna bandwidth via ground plane engineering [23]. Lightweight textile antennas have gained popularity, especially those using electrically conductive fabrics like Shielded Ripstop or Denim, due to their flexibility and thin profile — often around 1.6 mm. These materials are ideal for medical and athletic uses, where wearability, comfort, and bio-compatibility are critical [24], [25].

Due to their close interaction with human tissues, wearable antennas must be carefully evaluated for how mechanical bending or deformation influences both their electromagnetic behavior and biological safety. An essential factor in this context is the Specific Absorption Rate (SAR). To ensure user safety and minimize exposure risks, regulatory agencies have established SAR limits: the Federal Communications Commission (FCC) sets the maximum at 1.6 W/kg, while the International Commission on Non-Ionizing Radiation Protection (ICNIRP) allows up to 2 W/kg [26], [27].

The adverse effects arising from surface wave interference and rearward radiation directed into biological tissues can be effectively reduced through the use of metamaterial-based artificial ground structures [28]–[32]. These structures, particularly electromagnetic band-gap (EBG) configurations, replace traditional metallic grounds with textile-based layers composed of conductive and dielectric fabrics, offering enhanced compatibility with flexible systems.

This work introduces a thin, conformable dual-band textile antenna specifically engineered for biomedical environments, functioning at 2.45 GHz and 5.8 GHz, which are both within the ISM spectrum. The antenna's design integrates a T-shaped slot in the ground layer, which significantly improves electromagnetic consistency during on-body operation, while also ensuring compliance with SAR safety regulations. The study emphasizes the role of wearable antennas in health-related technologies, particularly how material characteristics influence antenna efficiency and reliability. Section II details the conceptual framework and progressive design methodology of a U-shaped dual-resonant antenna incorporating a T-slot structure. It further presents a comprehensive analysis of the S-parameter characteristics observed at various stages of the antenna's development process. Section

III investigates the influence of varying the spatial separation between the antenna structure and a modeled human arm on the antenna's radiative properties and impedance matching characteristics. It also includes SAR distribution assessments for both 1g and 10g tissue models at the operating frequencies. Finally, Section IV presents a comparative validation of the antenna design using simulated outputs from CST Studio Suite and COMSOL Multiphysics, demonstrating consistency across platforms.

II. METHODOLOGY

This study introduces a refined design based on the widely recognized dual-resonant U-shaped patch fabric antenna from [28], which is enhanced through the integration of an innovative T-shaped ground plane, as depicted in Figures 1(a) and 1(b). The U-shaped patch serves as a half-wavelength radiator, specifically tuned to operate at 2.45 GHz. The concept of resonant frequency is referenced from [33].

$$f_o = \frac{c}{2l\sqrt{\varepsilon_r}} \tag{1}$$

where c represents the speed of light, ε_r is the substrate's relative permittivity, and l denotes the length of the U-shaped radiating element. For primary resonance at 2.45 GHz, the length of the U-shaped patch, computed using Equation (1), measures 47.25 mm and consists of two distinct segments—29.5 mm and 17 mm—as depicted in Figure 1(a). To facilitate dual-band performance, a T-shaped slot is etched into the ground plane. This slot acts as a resonant structure operating at 5.8 GHz, with an effective electrical length of 19.95 mm, also derived from Equation (1). The slot's actual dimensions, totaling l=14 mm + 5 mm + 3 mm, are illustrated in Figure 1(b).

The electromagnetic response of the antenna was comprehensively characterized utilizing advanced full-wave electromagnetic simulation techniques within the CST Microwave Studio environment. validating its efficient dual-band performance centered at 2.45 GHz and 5.8 GHz-both within the ISM frequency range. Denim material is utilized as the substrate, characterized by a 0.7 mm thickness, ε_r of 1.68, and $tan(\delta)$ of 0.05. As shown in Figure 1, the antenna exhibits a miniaturized configuration, occupying a physical area of 40×13^2 mm². Shieldit Super, chosen for its excellent electrical conductivity of 5.8×10^7 S/m, forms the radiating and ground structures. The ground plane incorporates a dual T-shaped slot configuration interconnected by a metallized via to optimize antenna performance; this design enhances impedance matching and improves resonance characteristics across both operational frequency bands.

A. SIMULATION ENVIRONMENT

Wearable antennas demand specialized simulation environments that account for their close proximity and interaction with complex human tissues. They are significantly influenced by the electromagnetic properties of biological

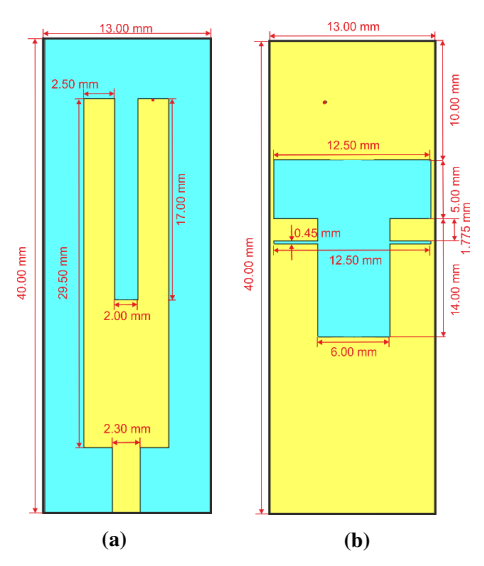


Figure 1. The Geometry of the proposed dual-resonance textile antenna:(a) front view [28], and (b) rear view.

materials, which can affect parameters such as impedance matching, resonance frequency, and radiation efficiency. To accurately assess their performance, these antennas must be tested under conditions that closely mimic real-world usage scenarios.

They are virtually positioned on various parts of the human body, to evaluate its behavior in realistic contexts. In this sstudy, and for simulation purposes, a multilayered phantom model was developed to replicate the anatomical structure of the human arm, as illustrated in Figure 2(a). This phantom comprises four distinct layers—bone, muscle, fat, and skin—each representing a specific tissue type with unique electromagnetic characteristics. Figure 2(b) presents the cross-sectional schematic of the modeled structure, while Table I outlines the detailed electrical and physical properties of each tissue layer, including relative permittivity, electrical conductivity, mass density, and thickness.

To precisely replicate the antenna's deployment on the human arm, the structure was conformally bent in CST Microwave Studio (CST MWS) to match the cylindrical geometry of a tissue-equivalent phantom with a diameter of 46 mm. This curvature emulates the natural anatomical contour of the arm, thereby incorporating mechanical deformation and its consequent influence on the antenna's electromagnetic behavior. Accurately assessing essential performance metrics—such as return loss, radiation efficiency, gain, radiation characteristics, and Specific Absorption Rate (SAR)—under realistic wearable usage scenarios requires conformal modeling, which plays a vital role in capturing the antenna's behavior in practical conditions.

By integrating anatomical realism into the simulation setup, this approach ensures that the antenna design is both practically viable and optimized for use in wearable healthcare, communication, or WBAN applications.

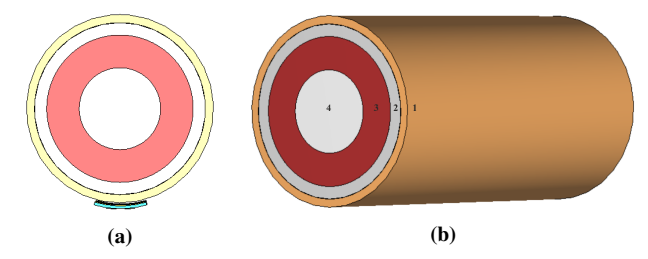


Figure 2. (a) Simulation setup, and (b) the four layers of the arm model.

Table 1: Electromagnetic and dielectric characteristics of the human arm tissue model [28], [34]

Layer	Thickness	Relative	Conductivity	Density
	Radius	Permittivity	$\sigma(S/m)$	(kg/m ³)
	(mm)	(ε_r)		
(1) Skin	2	38	1.46	1001
(2) Fat	3	5.28	0.1	900
(3) Muscle	8	52.72	1.73	1006
(4) Bone	10	18.54	0.8	1008

B. DESIGN PROCESS

The operational characteristics of a wearable antenna are significantly affected by multiple parameters arising from its close proximity and electromagnetic coupling with the human body, including dielectric loading, frequency detuning, and energy absorption losses. These influences necessitate a comprehensive and iterative design process to ensure the antenna meets both functional and performance requirements. In this work, the key design objectives are twofold: (1) to achieve reliable dual-frequency operation, and (2) to enhance impedance matching for minimal signal reflection and efficient radiation. To systematically achieve the desired objectives, the antenna configuration undergoes a six-step iterative development process, as depicted in Figure 3(a). The corresponding reflection coefficient (S11) for each design phase is presented in Figure 3(b), enabling a comparative assessment of performance enhancements throughout the progression.

• Design I – Flat Antenna without Ground The initial design iteration comprises a fundamental U-shaped radiating element situated on the substrate's top layer, with the bottom layer devoid of any conductive ground plane, as depicted in Figure 1(a. The antenna maintains a planar profile and is directly applied to the surface of a human arm model to replicate a realistic wearable application. This preliminary layout generates two separate resonant modes at 7.2 GHz and 9.35 GHz. However, both resonances exhibit inadequate impedance matching, which adversely affects the antenna's efficiency and narrows its operational bandwidth.

Design II – Flat Antenna with Full Ground
 To resolve the impedance mismatch issue, a continuous ground plane is implemented on the substrate's bottom layer, substituting the previous air-backed configuration



used in Design I. This alteration markedly influences the current flow and electromagnetic field distribution, resulting in a shift of the resonant frequencies to 3.95 GHz and 8 GHz. At these new frequencies, The antenna exhibits parallel resonance characteristics within the lower frequency band, while demonstrating series resonance behavior in the higher frequency band. While this adjustment enhances the overall response, additional refinement is necessary to align the resonance more closely with the targeted ISM frequency bands and to further optimize impedance matching.

- Design III Flat Antenna with T-Shaped Slot In this design phase, a T-shaped slot is incorporated into the ground plane to implement reactive loading, enabling precise adjustment of the antenna's frequency response. This slot functions as a perturbation element, altering the effective electrical length and creating new coupling interactions within the structure. Consequently, the fundamental resonance is reduced to 2.4 GHz, aligning with a widely used ISM band, while achieving better impedance matching. However, the higher-order resonance bifurcates and shifts to a lower frequency, reflecting substantial modifications in current distribution and mode dynamics.
- Design IV Flat Antenna Incorporating a T-Shaped Slot and Conductive Via To improve impedance matching and exert more precise control over the antenna's dual-resonant characteristics, a conductive via is added to connect the bottom ground plane with the upper U-shaped radiating element. Placed strategically at the midpoint of the patch's right arm, this via acts as an inductive loading component. This adjustment causes the primary resonance to shift slightly upward to 2.6 GHz, while the secondary resonance moves to 6.14 GHz. Moreover, incorporating the via markedly enhances impedance matching at both resonant frequencies, resulting in a more stable and optimized antenna performance within the designated ISM bands.
- Design V Curved Antenna with T-Shaped Slot and Via Recognizing the conformal nature of wearable antennas when integrated with the human body, the previously planar design is subsequently bent to align with the cylindrical geometry of a human arm, modeled with a diameter of 46 mm. This mechanical deformation induces additional electromagnetic coupling effects arising from the curvature. Notably, the fundamental resonant frequency remains largely unaffected, whereas the higher-order resonance exhibits a downward shift to 5.88 GHz, accompanied by enhanced impedance matching. The performance enhancement is primarily driven by the strengthened capacitive interaction between the antenna design and the tissue-representative phantom material, which effectively modifies the near-field interaction and resonance characteristics.
- Design VI Curved Antenna with Dual Overlapping T-

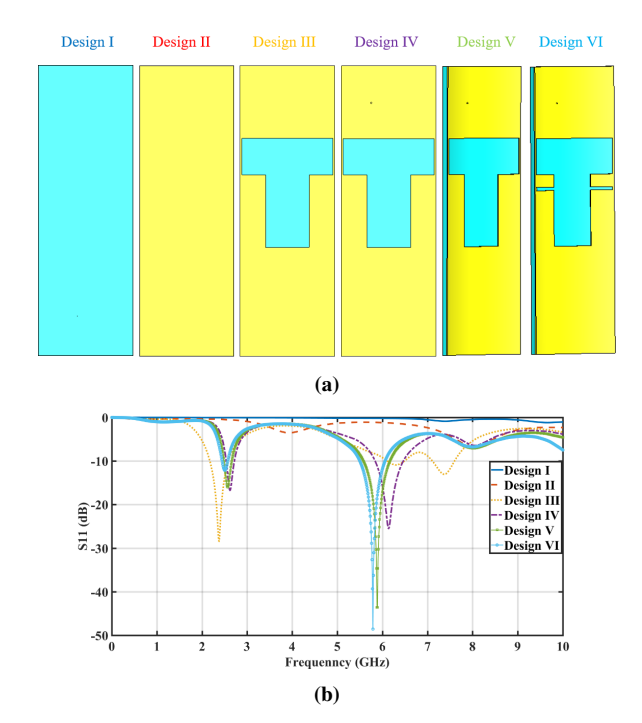


Figure 3. (a) Evolution of the proposed dual-resonance antenna, and (b) the reflection coefficient for each design.

Shaped Slots and Via

In the final design iteration, the ground plane is further refined by replacing the single T-shaped slot with two overlapping T-shaped slots, enabling more precise tuning of the resonant frequencies. Incorporating overlapping slots into the ground structure adds complexity to the reactive loading mechanism, providing enhanced control over the surface current flow. This structural refinement facilitates precise alignment of the antenna's resonant modes with the target ISM frequencies of 2.45 GHz and 5.8 GHz. At both bands, the antenna achieves reflection coefficients below $-10~{\rm dB}$, indicating strong impedance matching. The resulting design delivers a high-efficiency, dual-band wearable antenna that maintains stable performance even in the presence of human-body-induced electromagnetic effects.

III. SIMULATION RESULTS

A. IMPACTS OF ARM LOADING

The developed dual-band textile antenna is precisely designed to ensure high-efficiency operation at 2.45 GHz and 5.8 GHz, even under close proximity to the biological tissue structure, specifically the forearm region. As illustrated in the simulation configuration in Figure 2, the antenna is conformally placed on a multilayer anatomical arm phantom that replicates the electromagnetic properties and stratified composition of biological tissues, including epidermis, adipose tissue, musculature, and osseous structures. This anatomically accurate phantom is critical due to the elevated dielectric constants and conductivities of these tissues, as de-

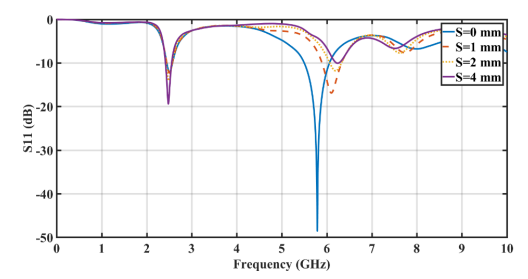


Figure 4. Variation in return loss relative to the antenna's spacing from the tissue-equivalent phantom.

tailed in Table I, which significantly influence the antenna's resonant characteristics and impedance response.

To thoroughly examine the interaction between the antenna and surrounding biological materials, an extensive parametric study was conducted. This involved systematically altering the distance between the antenna and the arm phantom to evaluate how varying proximity influences electromagnetic performance. This approach allows for the investigation of performance variations under different mounting scenarios-ranging from direct skin contact to slightly elevated placements (e.g., due to clothing or padding). The simulation results, presented in Figure 4, reveal that the resonant frequency near 5.8 GHz is highly sensitive to the antenna's distance from the arm. As the distance increases, this higherfrequency resonance shifts upward, and the impedance matching deteriorates, indicating reduced coupling efficiency and possible detuning effects caused by the reduced dielectric loading.

Conversely, the lower-frequency resonance at 2.45 GHz exhibits greater stability across varying distances. While the resonant frequency remains largely unchanged, the impedance matching shows noticeable improvement as the antenna moves farther from the arm. This suggests that the lower band is less affected by minor variations in dielectric environment and benefits from reduced tissue-induced loss when slightly offset from the skin.

These findings underscore the critical importance of accounting for antenna-body electromagnetic coupling during the design and implementation of wearable antennas. They further elucidate the inherent trade-off between resonance stability induced by proximity effects and radiation efficiency, particularly in dual-band configurations. Ultimately, this analysis validates the design's resilience and consistent performance under realistic operational scenarios, where variations in antenna placement may occur due to factors such as user motion, garment layering, or integration techniques.

B. SPECIFIC ABSORPTION RATE EVALUATION

The Specific Absorption Rate (SAR) quantifies the rate at which radiofrequency (RF) electromagnetic energy is deposited in biological tissues, typically represented in units of watts per kilogram (W/kg). This metric is crucial for assessing the biological safety of devices emitting electromagnetic

radiation. SAR can be calculated either over small localized tissue volumes or averaged across larger masses to evaluate compliance with established safety standards. Two widely recognized regulatory guidelines define acceptable SAR levels: IEEE C95.1-1999 enforces a limit of 1.6 W/kg averaged over 1 gram of tissue [35], while IEEE C95.1-2005 permits up to 2 W/kg averaged across 10 grams [36]. Variations also exist in how different organizations define the averaging region; for instance, the FCC applies a 1 g average [37], whereas ICNIRP adopts a 10 g standard [38]. To comply with these safety regulations, wearable antenna systems must function at strictly regulated power outputs. Figure 5(a) illustrates the distribution of SAR averaged over 1 gram of tissue on a human arm phantom (top view), exposed to a 2.45 GHz field at an input power level of 10 mW. The peak SAR values (highlighted in red) are concentrated centrally, indicating the region of maximal RF energy absorption. It reaches approximately 1.18 W/kg, which demonstrates that the antenna operates well within safe exposure limits while maintaining efficient energy utilization. Figure 5(e) represents the side view of the 1g-SAR distribution at the same frequency and accepted power. It shows that the highest SAR values are concentrated in the first two layers of the arm model and start to diminish as you move more inside the deep layers. Figure 5(b) represents the 1g-SAR distribution on the human arm model (top view) when exposed to an electromagnetic field at 5.8 GHz with an accepted power of 10 mW. The peak recorded SAR value is around 1.44 W/kg, which remains within the permissible threshold defined by regulatory safety standards. Figure 5(f) represents the side view of the 1g-SAR distribution at the same frequency and accepted power. The same observation was replicated, as seen in the case of 1g-SAR at 2.45 GHz. Figure 5(c) represents the 10g-SAR distribution on the human arm model (top view) when exposed to an electromagnetic field at 2.45 GHz with an accepted power of 50 mW. The highest SAR values reach approximately 1.64 W/kg, which demonstrates the design's compliance with electromagnetic exposure guidelines. Figure 5(g) represents the side view of the 10g-SAR distribution at the same frequency and accepted power. It represents the energy absorption profile within the human arm model. The SAR decay pattern was observed starting in the third layer and diminishing in the last layer. Figure 5(c) represents the 10g-SAR distribution on the human arm model (top view) when exposed to an electromagnetic field at 5.8 GHz with an accepted power of 50 mW. The highest SAR values reach approximately 2 W/kg, indicating compliance with safety standards. Figure 5(h) represents the side view of the 10g-SAR distribution at the same frequency and accepted power. It shows almost the same energy absorption profile as seen in the case of 10g-SAR at 2.45 GHz.

IV. DESIGN VALIDATION

A. S-PARAMETER CHARACTERISTICS

To ensure the robustness and validity of the simulation outcomes obtained via CST Microwave Studio (CST MWS),

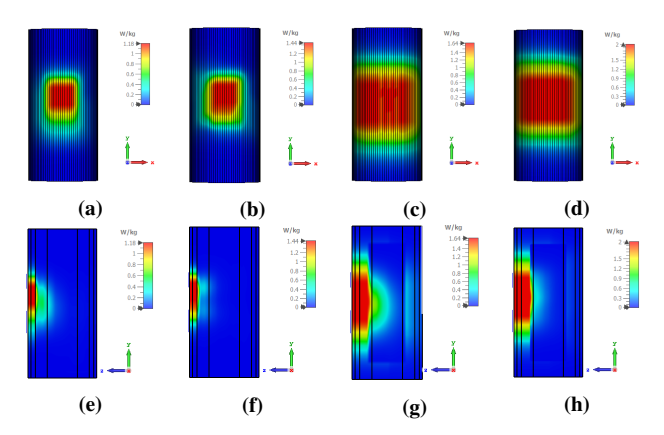


Figure 5. SAR distribution of the dual-resonance fabric antenna at: (a) 1g-SAR at 2.45 GHz (top view), (b) 1g-SAR at 5.8 GHz (top view), (c) 10g-SAR at 2.45 GHz (top view), (d) 10g-SAR at 5.8 GHz (top view), (e) 1g-SAR at 2.45 GHz (side view), (f) 1g-SAR at 5.8 GHz (side view), (g) 10g-SAR at 2.45 GHz (side view), and (h) 10g-SAR at 5.8 GHz (side view).

a cross-validation analysis was conducted by benchmarking the results against those produced using COMSOL Multiphysics. This comparative analysis confirms the reproducibility and robustness of the antenna's electromagnetic performance predictions across multiple full-wave simulation tools, thereby reinforcing the validity and precision of the simulated results.

Figure 6 illustrates the reflection coefficient (S11) outcomes derived from both CST and COMSOL simulation platforms. The results exhibit strong agreement, especially in identifying the antenna's dual-resonant behavior. This alignment confirms the antenna's ability to maintain its intended operational frequencies—2.45 GHz and 5.8 GHz—regardless of the simulation tool utilized.

Specifically, the CST simulation indicates reflection coefficients of approximately –10.23 dB at 2.45 GHz and –36 dB at 5.8 GHz, reflecting excellent impedance matching at the higher band and satisfactory performance at the lower one. Meanwhile, the COMSOL output yields values of –14.69 dB at 2.45 GHz and –14.97 dB at 5.8 GHz. The observed discrepancies in magnitude stem from variations in solver techniques, boundary condition configurations, and meshing strategies used by each platform. Despite these minor differences, both simulation tools consistently identify the same resonant frequencies and confirm effective impedance matching.

This comparative validation not only confirms the antenna's dual-band performance but also demonstrates the robustness of the design across different electromagnetic solvers. Such consistency is crucial when transitioning from simulation to prototyping and experimental testing, as it reduces uncertainty in performance predictions and enhances the credibility of the design process.

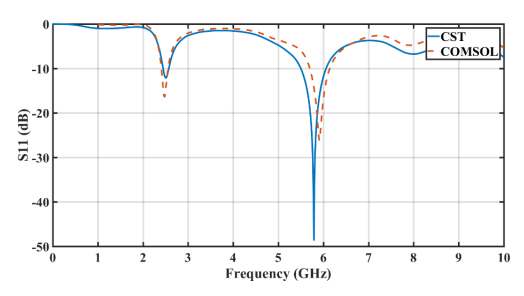


Figure 6. Reflection coefficient variation with respect to the separation distance from the phantom.

B. RADIATION PATTERNS

The performance of any wireless communication system is fundamentally influenced by its antennas radiation patterns. Figure 7 presents the radiation characteristics for different antenna configurations. When operating in free space at 2.45 GHz, the standalone antenna exhibits a radiation behavior similar to that of a classic dipole, producing an almost omnidirectional field distribution, as shown in Figures 7(a) and 7(b). In contrast, at 5.8 GHz, the antenna generates a more directional, bidirectional pattern, clearly illustrated in Figures 7(c) and 7(d).

Once the antenna is positioned in close proximity to the tissue-mimicking phantom—simulating real-world on-body conditions—its radiation pattern at 2.45 GHz becomes more directional, as depicted in Figures 7(a) and 7(b). Achieving efficient radiation in this scenario is inherently difficult, largely due to substantial energy absorption by the high-permittivity, lossy biological materials within the phantom. Under these conditions, the radiation efficiency is reduced, averaging around –10.5 dB, equivalent to approximately 8.9%. At 5.8 GHz, the antenna continues to exhibit a directive radiation pattern; however, both the E-plane and H-plane show increased distortion, leading to a less consistent angular radiation profile, as seen in Figures 7(c) and 7(d). The efficiency drops further at this frequency, reaching roughly –15.6 dB, or about 2.7%.

To confirm the accuracy of the radiation pattern data generated by CST Microwave Studio, complementary electromagnetic simulations were performed using COMSOL Multiphysics. The comparative analysis presented in Figure 7 demonstrates strong concordance between the radiation characteristics predicted by both simulation platforms, confirming the reliability of the modeling approach.

V. CONCLUSION

This study introduces a miniaturized and conformable dualband antenna specifically designed for integration within wearable biomedical systems, operating at 2.45 GHz and 5.8 GHz within the ISM frequency range. Utilizing a novel U-shaped radiating patch combined with a T-shaped slotted ground plane, the antenna was constructed on a denim substrate with Shieldit Super conductive fabric. This design ensured strong impedance matching, consistent radiation char-

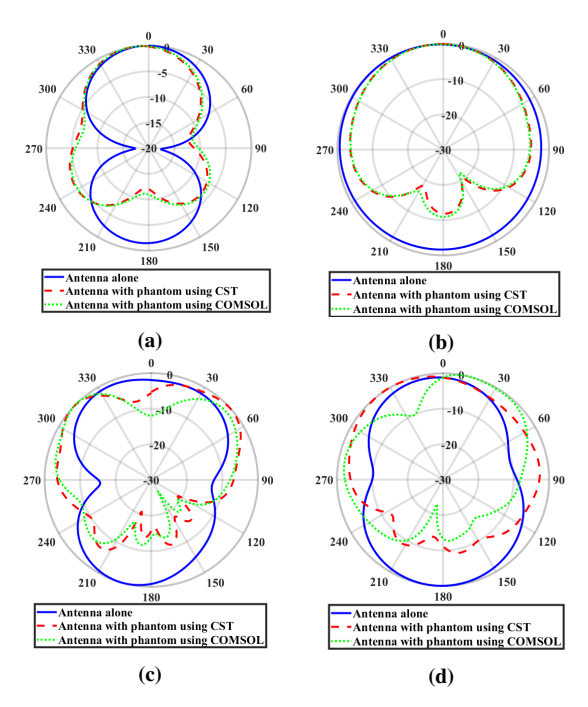


Figure 7. Simulated radiation pattern profiles depicting (a) the E-plane at 2.45 GHz, (b) the H-plane at 2.45 GHz, (c) the E-plane at 5.8 GHz, and (d) the H-plane at 5.8 GHz.

acteristics, and adherence to SAR safety limits, recording values of 1.18 W/kg at 2.45 GHz and 1.44 W/kg at 5.8 GHz based on 1-gram tissue averaging. Through a systematic optimization process—including the integration of vias, structural bending, and overlapping slot features—the antenna exhibited robust performance against body-induced loading effects, sustaining its functionality over varying proximities to the human arm.

Simulations in CST Microwave Studio and COMSOL Multiphysics validated the design's dual-band operation, with reflection coefficients below -10 dB at both frequencies. Radiation patterns transitioned from omnidirectional (free space) to directive (on-body), albeit with reduced efficiency (-10.5 dB at 2.45 GHz, -15.6 dB at 5.8 GHz) due to tissue absorption. SAR analysis confirmed adherence to IEEE, FCC, and ICNIRP guidelines, ensuring safe integration into WBANs for healthcare, sports, and military applications.

Future work could explore miniaturization, multi-band expansion, and experimental validation under dynamic conditions (e.g., movement, moisture). This antenna's low-profile, textile-based design addresses critical challenges in wearable technology, balancing performance, safety, and user comfort for next-generation BCC systems.

ACKNOWLEDGMENT

This research was carried out within the Department of Electrical Engineering, Faculty of Engineering, at Applied Science Private University, Amman, Jordan. The authors gratefully acknowledge the university's substantial support and resources that facilitated the successful completion of this study.

References

- Mersani A, Osman L, Ribero JM. Flexible UWB AMC antenna for early stage skin cancer identification. Progress In Electromagnetics Research M. 2019:80:71-81.
- [2] Al Rasyid MU, Lee BH, Sudarsono A. Wireless body area network for monitoring body temperature, heart beat and oxygen in blood. In international seminar on intelligent technology and its applications (ISITIA) 2015: 05-08
- [3] Nie HK, Xuan XW, Ren GJ. Wearable antenna pressure sensor with electromagnetic bandgap for elderly fall monitoring. AEU-International Journal of Electronics and Communications. 2021;138:153861.
- [4] Wang Y, Shi J, Wang J. Wearable antenna sensor based on EBG structure for human body area humidity monitoring. IEEE Sensors Journal. 2023;24(3):3833-43.
- [5] Saleh GS, inventor; Imam Abdulrahman Bin Faisal University, assignee. Dual resonant wearable antenna. United States patent US 11,870,135. 2024 Jan 9.
- [6] Saleh G. Dual resonant wearable metamaterial for medical applications. Int. J. Commun. Antenna Propag. 2021;11:85-93.
- [7] Dandal FH, AL-Qahtani MM, AL-Harbi MA, Alessa ES, Aljamaan I, Saleh G. Aerobic Athletes Tracking System Using Smart Glove for Physiological and Kinematic Monitoring. In 2024 International Conference on Engineering and Emerging Technologies (ICEET) 2024: 1-6.
- [8] Technical and operating parameters and spectrum use for short-range radiocommunication devices, International Telecommunication Union. [Online]. Available: http://www.itu.int/pub/R-REP-SM.2153-2-2011
- [9] ETSI EN 301839-1, European Telecommunications Standards Institute, 2007. [Online]. Available: http://www.etsi.org/deliver/etsi_en/301800_301899/30183901/01.03.01_60/en_30183
- [10] Federal Communications Commission, 47 CFR part 95. [Online]. Available: https://www.fcc.gov/wireless/bureau-divisions/mobility-division/wireless-medical-telemetry-service-wmts
- [11] Kiourti A. Between telemetry: Communication between implanted devices and the external world. Opticon1826. 2010; 1(8).
- [12] Furse CM. Biomedical telemetry: Today's opportunities and challenges. In2009 IEEE International Workshop on Antenna Technology 2009: 1-4.
- [13] Giftsy AS, Kommuri UK, Dwivedi RP. Flexible and wearable antenna for biomedical application: progress and opportunity. IEEE Access. 2023;12:90016-40.
- [14] Memarzadeh-Tehran H, Abhari R, Niayesh M. A cavity-backed antenna loaded with complimentary split ring resonators. AEU-International Journal of Electronics and Communications. 2016;70(7):928-35.
- [15] Muhammad Z, Shah SM, Abidin ZZ, Asyhap AY, Mustam SM, Ma Y. CPW-fed wearable antenna at 2.4 GHz ISM band. InAIP Conference Proceedings 2017; 1883(1).
- [16] Yan S, Soh PJ, Vandenbosch GA. Wearable dual-band magneto-electric dipole antenna for WBAN/WLAN applications. IEEE Transactions on antennas and propagation. 2015;63(9):4165-9.
- [17] Ma L. On-body flexible printed antennas for body-centric wireless communications. (Doctoral dissertation, Loughborough University, 2009).
- [18] Chan KH, Fung LC, Leung SW, Siu YM. Effect of internal patch antenna ground plane on SAR. In2006 17th International zurich symposium on electromagnetic compatibility 2006:513-516.
- [19] Tubbal FE, Raad R, Chin KW. A survey and study of planar antennas for pico-satellites. IEEE Access. 2015;3:2590-612.
- [20] Abulgasem S, Tubbal F, Raad R, Theoharis PI, Lu S, Iranmanesh S. Antenna designs for CubeSats: A review. IEEE access. 2021;9:45289-324.
- [21] Musa U, Shah SM, Majid HA, Mahadi IA, Rahim MK, Yahya MS, Abidin ZZ. Design and analysis of a compact dual-band wearable antenna for WBAN applications. IEEE Access. 2023;11:30996-1009.
- [22] Gao GP, Zhang BK, Dong JH, Dou ZH, Yu ZQ, Hu B. A compact dual-mode pattern-reconfigurable wearable antenna for the 2.4-GHz WBAN application. IEEE Transactions on Antennas and Propagation. 2022;71(2):1901-6.
- [23] Sukhija S, Sarin RK. A U-shaped meandered slot antenna for biomedical applications. Progress In Electromagnetics Research M. 2017;62:65-77.
- [24] Le TT, Yun TY. Miniaturization of a dual-band wearable antenna for WBAN applications. IEEE Antennas and Wireless Propagation Letters. 2020;19(8):1452-6.



- [25] Smida A, Iqbal A, Alazemi AJ, Waly MI, Ghayoula R, Kim S. Wideband wearable antenna for biomedical telemetry applications. IEEE Access. 2020;8:15687-94
- [26] Zahran SR, Abdalla MA, Gaafar A. New thin wide-band bracelet-like antenna with low SAR for on-arm WBAN applications. IET Microwaves, Antennas & Propagation. 2019;13(8):1219-25.
- [27] Ali U, Ullah S, Shafi M, Shah SA, Shah IA, Flint JA. Design and comparative analysis of conventional and metamaterial-based textile antennas for wearable applications. International Journal of Numerical Modelling: Electronic Networks, Devices and Fields. 2019;32(6).
- [28] Ashyap AY, Zainal Abidin Z, Dahlan SH, Majid HA, Saleh G. Metamaterial inspired fabric antenna for wearable applications. International Journal of RF and Microwave Computer-Aided Engineering. 2019;29(3).
- [29] Gao GP, Hu B, Wang SF, Yang C. Wearable circular ring slot antenna with EBG structure for wireless body area network. IEEE Antennas and Wireless Propagation Letters. 2018;17(3):434-7.
- [30] Ashyap AY, Elamin NI, Dahlan SH, Abidin ZZ, See CH, Majid HA, Al-Fadhali N, Mukred JA, Saleh G, Esmail BA. Via-less electromagnetic band-gap-enabled antenna based on textile material for wearable applications. PLoS One. 2021;16(1).
- [31] Chen YS, Ku TY. A low-profile wearable antenna using a miniature high impedance surface for smartwatch applications. IEEE Antennas and Wireless Propagation Letters. 2015;15:1144-7.
- [32] Ashap AY, Abidin ZZ, Dahlan SH, Majid HA, Yee SK, Saleh G, Malek NA. Flexible wearable antenna on electromagnetic band gap using PDMS substrate. TELKOMNIKA (Telecommunication Computing Electronics and Control). 2017;15(3):1454-60.
- [33] Balanis CA. Antenna theory: analysis and design. John wiley & sons; 2016.
- [34] NR WA, Abdirahman MS. Performance of ultra-wideband wearable antenna under severe environmental conditions and specific absorption rate (SAR) study at near distances. ARPN Journal of Engineering and Applied Sciences 2006.
- [35] IEEE Standards Coordinating Committee 2. IEEE standard for safety levels with respect to human exposure to radio frequency electromagnetic fields, 3kHz to 300GHz. IEEE C95. 1-1991. 1992.
- [36] IEEE Standards Coordinating Committee 2. IEEE standard for safety levels with respect to human exposure to radio frequency electromagnetic fields, 3kHz to 300GHz. IEEE C95. 1-1991. 2005.
- [37] Fields RE. Evaluating compliance with FCC guidelines for human exposure to radiofrequency electromagnetic fields. Oet Bull. 1997;65(10):1-57.
- [38] FIELDS ET. GUIDELINES FOR LIMITING HUMAN EXPOSURE TO ELECTROMAGNETIC FIELDS UP TO 300 GHz. 2009